APPLIED PHYSICS LETTERS **107**, 091107 (2015)

Coherent phonon spectroscopy of non-fully symmetric modes using resonant terahertz excitation

T. Huber,[1,a)] M. Ranke,[2] A. Ferrer,[1,3] L. Huber,[1] and S. L. Johnson[1]
[1]*Institute for Quantum Electronics, Physics Department, ETH Zurich, CH-8093 Zurich, Switzerland*
[2]*The Hamburg Centre for Ultrafast Imaging, Luruper Chaussee 149, D-22761 Hamburg, Germany*
[3]*Swiss Light Source, Paul Scherrer Institut, CH-5232 Villigen PSI, Switzerland*

(Received 10 July 2015; accepted 20 August 2015; published online 1 September 2015)

We use intense terahertz (THz) frequency electromagnetic pulses generated via optical rectification in an organic crystal to drive vibrational lattice modes in single crystal Tellurium. The coherent modes are detected by measuring the polarization changes of femtosecond laser pulses reflecting from the sample surface, resulting in a phase-resolved detection of the coherent lattice motion. We compare the data to a model of Lorentz oscillators driven by the near-single-cycle broadband THz pulse. The demonstrated technique of optically probed coherent phonon spectroscopy with THz frequency excitation could prove to be a viable alternative to other time-resolved spectroscopic methods like standard THz time domain spectroscopy. © *2015 AIP Publishing LLC*.
[http://dx.doi.org/10.1063/1.4930021]

Coherent phonon spectroscopy has emerged as a widely practiced method for investigating phenomena connected with low-frequency vibrational dynamics in solids. It has, for example, proven to be a powerful tool in the study of broken symmetry ground states and the investigation of coupling between the lattice and other degrees of freedom in a solid.[1–7] In a typical coherent phonon spectroscopy experiment, a short-pulse laser with a center frequency in the visible or near-infrared region of the spectrum drives a vibrational coordinate via a Raman process. For solids with a bandgap larger than the photon energy of the excitation pulse, the coupling to vibrational states occurs via short-lived virtual electronic states and produces very small amplitude coherent motion. Anharmonic coupling of lattice modes to a coherent phonon can however only be studied in the large amplitude limit of the coherent motion. Above-bandgap excitation can lead to a stronger coupling to certain modes since the excited states are real and have a much longer effective lifetime.[8,9] Although the amplitude of coherent motion from above-bandgap excitation can be up to several pm, this also leads to a highly non-equilibrium electron population and subsequent electronic relaxation processes. This ultimately presents a limitation for scaling up such processes to achieve large-scale coherent motions due to a large increase in sample temperature or even sample damage. Measured damping times can furthermore be influenced by a coupling of phonon modes to the optically excited carrier plasma.

An alternative approach to driving coherent excitations with an associated electric dipole moment is to use low-frequency radiation to couple directly to the dipole moment of the vibration. This requires strong sources of phase-stable coherent electromagnetic radiation with significant spectral content in the range of 1–50 THz, the typical range of frequencies for vibrational excitations found in condensed matter systems. Recent advances in the generation of intense terahertz (THz) frequency electromagnetic pulses[10,11] with significant spectral components in the low THz range (around 1–5 THz) have facilitated the dipole excitation of lower-frequency excitations in solids. Intense THz pulses have, for example, been used to coherently control antiferromagnetic spin waves[12] and to drive spin dynamics associated with an electromagnon.[13]

The direct interaction of phase-stable THz frequency pulses with polar optical lattice modes in solids has so far been investigated with THz time domain spectroscopy (TDS),[14] where spectral changes of a THz pulse after interaction with a sample are investigated. This approach becomes increasingly difficult for materials that are strongly absorbing in the THz range, an inherent characteristic of systems with excitations featuring strong THz resonances. In that case, TDS measurements have to be carried out in reflection geometry and sample quality and positioning become challenging for a reliable measurement.[15] The sample surface needs to be flat and homogeneous for at least the diameter of the THz spot—already step heights of 1 μm can introduce significant phase error.

In this letter, we present an alternative method of time-resolved coherent phonon spectroscopy using resonant THz excitation of infrared active lattice modes, demonstrated in single crystal Tellurium (Te). Intense THz frequency pulses are generated via optical rectification of a near-infrared femtosecond laser pulse in an organic 4-N,N-dimethylamino-4$'$-N$'$-methyl-stilbazolium 2,4,6-trimethylbenzenesulfonate (DSTMS) crystal.[11,16] Anisotropic reflectivity changes associated with lattice vibrations are probed with optical femtosecond laser pulses, enabling us to phase-resolve the coherent motion. The method allows us to infer properties of a large-amplitude coherent phonon without exciting free carriers in the system and to connect the observed reflectivity change to the applied electric field. We model the system as a collection of damped harmonic oscillators driven by the field of the THz pulse, an approach that allows the study of strongly damped lattice modes.

Tellurium is a semiconductor with a narrow bandgap of 0.33 eV and has spacegroup $P3_121$ ($P3_221$).[17,18] The

---

[a] Electronic mail: tihuber@phys.ethz.ch

© 2015 AIP Publishing LLC

primitive unit cell contains three atoms arranged in a helix around the c-axis. The occurrence of polar phonon modes in elemental Te can be explained by a rearrangement of electronic charge during vibration.[19] Tellurium hosts six optical eigenmodes at the Γ-point of the Brillouin zone. One such mode is a fully symmetric, Raman active A_1-mode (3.6 THz). There is also a degenerate pair of infrared (IR) active modes that split into a transverse optical (TO) and longitudinal optical (LO) phonon mode ($A_{2,\mathrm{TO/LO}}: 2.6/2.82\,\mathrm{THz}$, internal polarization $E \parallel c$). The remaining non-fully symmetric modes are degenerate and both IR and Raman active ($E'_{\mathrm{TO/LO}}: 2.76/3.09\,\mathrm{THz}$ and $E''_{\mathrm{TO/LO}}: 4.22/4.26\,\mathrm{THz}$, internal polarization $E \perp c$). The atomic displacements associated with the E_{TO}-modes lie in a plane perpendicular to the c-axis (see Fig. 2(b)). In the past, different mechanisms arising from above-bandgap excitation with femtosecond laser pulses (deformation potential coupling[1,20] and the ultrafast buildup of a photo-Dember field[21]) have been exploited to coherently excite both the A_1 breathing mode as well as the non-fully symmetric E-modes. In these experiments, high transient concentrations of free carriers and the resulting changes in electronic bonds can lead to a considerable amount of softening of the A_1 mode frequency, while the reflectivity changes associated with the excited E-modes are nearly two orders of magnitude smaller compared to the A_1 mode amplitude.[1,21] In a reconstruction of the femtosecond motion of all atoms in a Te unit cell after photoexcitation with time-resolved x-ray diffraction, no signature of modes with E-symmetry could be observed.[22] The fact that the E-modes are both Raman and IR active allows for a scheme of direct excitation with a THz pulse and femtosecond optical detection. The Raman tensor associated with E-modes contains off-diagonal elements, which can be accessed measuring the anisotropic reflectivity changes after THz excitation.[17,21]

For the experiment, we used a Ti:Sapphire laser system that outputs pulses with a full-width-half-maximum duration (FWHM) $t_0 = 90\,\mathrm{fs}$ and a wavelength $\lambda_L = 800\,\mathrm{nm}$ at a repetition rate of 1 kHz. The pulses are split into a probe branch (around 1 μJ pulse energy) and a pump branch (8 mJ pulse energy) that is sent into a high-energy optical parametric amplifier (OPA). The OPA was set to generate 1.4 mJ pulses with a FWHM pulse length $t_{\mathrm{OPA}} = 80\,\mathrm{fs}$ at a wavelength $\lambda_{\mathrm{OPA}} = 1450\,\mathrm{nm}$. The experimental setup is shown in Fig. 1(a).

THz frequency pulses are generated in a DSTMS crystal via optical rectification[11,16] of the OPA pulses. The OPA beam is collimated onto the 590 μm thick DSTMS crystal with a spot size slightly smaller than the 6 mm diameter aperture of the crystal. The OPA beam is modulated with a chopper ($f = 500\,\mathrm{Hz}$) in order to increase signal-to-noise ratio of the measured delay traces and to reduce the thermal load on the generation crystal. After the crystal, a lowpass filter (Teflon) blocks residual infrared radiation before the polarization of the THz is set by a wiregrid polarizer. The entire THz beam path is enclosed and purged with N_2 to reduce the effects of water absorption lines in the spectrum of the THz pulse. THz radiation is focused on the sample by an off-axis parabolic mirror (focal length 101.6 mm) to a $1/e^2$ spot size of 600 μm, as measured with a microbolometer array camera. The probe beam is focused onto the sample through a hole in the parabolic mirror to a $1/e^2$ spot size of 150 μm, ensuring we probe a laterally homogeneously excited sample. The polarization of the probe beam is set with a thin film polarizer, the relative time delay between THz pump and 800 nm probe pulses can be varied by a motorized delay stage.

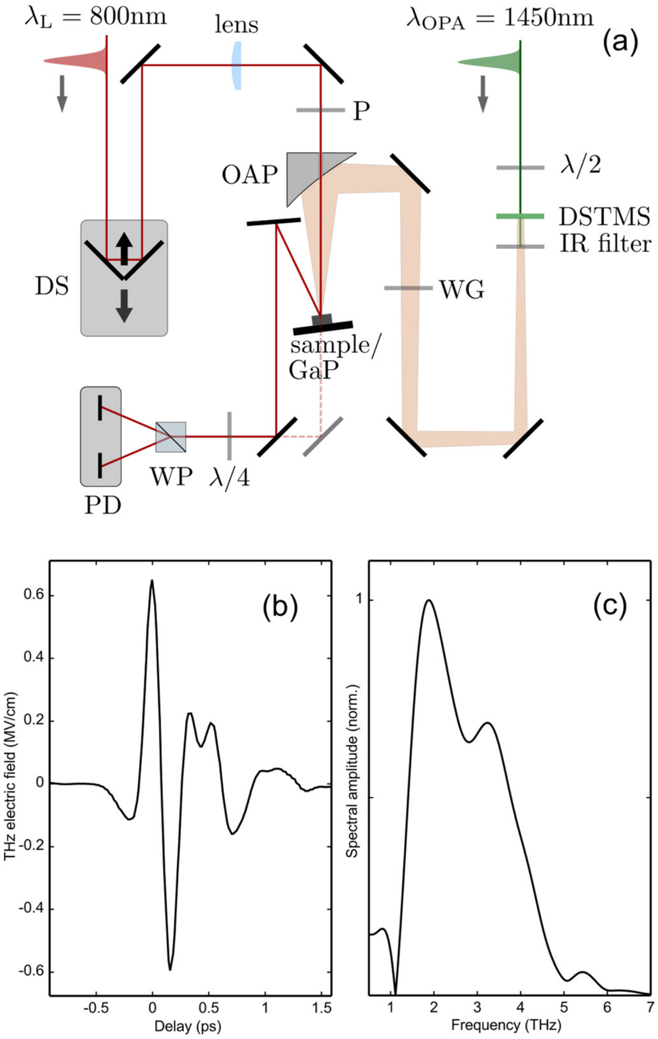

FIG. 1. (a) Experimental setup. DS: delay stage, OAP: off axis parabolic mirror, PD: balanced photodiode, WG: wiregrid polarizer, P: thin film polarizer, WP: Wollaston prism. Measurements on Te samples are performed in a reflection geometry. The dashed line after the sample corresponds to the beam path after the sample is replaced by a GaP crystal, which allows to characterize THz pulses via EO sampling without changing the pump arm. (b) Electric field of the THz pulse at the sample position measured with EO sampling in a GaP crystal. The field strength is calculated as described in the text. (c) Spectral amplitude obtained from the EO trace.

The geometry of the setup allows for easy switching between two measurement modes: (1) characterization of THz pump pulses via standard electro-optic (EO) sampling in transmission, and (2) reflection measurements on a Te sample without changing the pump arm. This is done by simply replacing one mirror in the probe arm. Figure 1(b) shows an EO trace measured at the sample position. EO sampling measurements are carried out with a $L = 100\,\mu\mathrm{m}$ thick (110)-GaP crystal. The field strength E_{THz} is estimated using the connection between E_{THz} and the transient induced change in birefringence of the crystal, given by[23] $E_{\mathrm{THz}} = (\lambda_L \sin^{-1}((I_1 - I_2)/(I_1 + I_2))/(2\pi L r_{41} n_0^3 t_{\mathrm{GaP}})$. Here, I_1 and

I_2 are the intensities of two orthogonal polarization channels separated by a Wollaston prism and measured with a balanced photodiode, $n_0 = 3.2$ is the refractive index of GaP for the probe wavelength,[24] $r_{41} = 0.88\,\mathrm{pm/V}$ is the EO coefficient of GaP,[25] and $t_{\mathrm{GaP}} = 0.46$ is the transmission coefficient of GaP for the center frequency of the THz pulses.[26] The peak signal of the measured THz trace corresponds to a modulation $(I_1 - I_2)/(I_1 + I_2) = 0.63 \pm 0.02$, amounting to a field strength $E_{\mathrm{THz}}^{\mathrm{peak}} = 0.64 \pm 0.02\,\mathrm{MV/cm}^2$.[27] Figure 1(c) shows the corresponding spectral amplitude, which is centered around $\nu = 2.6\,\mathrm{THz}$ and has a FWHM bandwidth $\Delta\nu = 2.4\,\mathrm{THz}$, providing enough spectral range to excite all infrared active phonon modes in Te.

The THz pump and near-infrared probe pulses hit the (001)-Te sample at an incidence angle of 5°, ensuring only a small deviation from the condition $E_{\mathrm{THz}} \perp c$ required for excitation of the E-modes. The probe pulses are reflected from the Te sample and guided to the balanced photodiodes. To detect a change in susceptibility caused by an atomic displacement associated with one of the E modes, we measure the anisotropic reflectivity changes at varying time delays after THz excitation.[21] As with EO sampling, the signal $\Delta R = R_1 - R_2$ is proportional to the difference of two orthogonal polarization channels separated by the Wollaston prism. Fig. 2(a) shows the time evolution of the measured signal $\Delta R/R_0$ with the polarization of THz pump and probe set as shown in Fig. 2(b). We observe a clear oscillatory signature of resonantly driven lattice modes, indicating that more than one mode is excited by the near-single-cycle broadband THz spectrum. Note that we do not observe any relaxation dynamics related to electron-electron scattering or electron-hole recombination. This is expected since the energy of photons in the THz pump pulse is much smaller than the bandgap of Te, making a promotion of electrons into the conduction band highly unlikely. Even in the event that some electron hole pairs are excited, their contributions to the anisotropic component of the reflectivity are expected to be negligible. Additional measurements of the isotropic reflectivity after THz excitation did not show any changes above the noise level $\sim 0.5 \times 10^{-3}$.

To analyze the signal, we consequently do not take into account any electronic background processes. For the presented THz driving field with a peak signal $E_{\mathrm{THz}}^{\mathrm{peak}} \approx 0.6\,\mathrm{MV/cm}$, we observe an anisotropic reflectivity change $\Delta R/R_0$ close to $3 \cdot 10^{-3}$. Obtaining a comparable signal level $(\Delta R/R_0 > 10^{-3})$ from E modes using above-bandgap excitation of Te would lead to a significant concentration of free carriers[1,21] and A_1 mode softening.

Figure 2 shows the spectral amplitude of the measured signal, displaying strong peaks at the frequencies of the E_{TO} modes. The measured lattice resonances exhibit features that are not measured in more conventional coherent phonon measurements with a high-frequency pump. Initially, the coupling of the IR active lattice modes to the driving field E_{THz} leads to broad shoulders in the spectral amplitude of the signal. These far-from-resonance contributions damp out quickly once $E_{\mathrm{THz}} \approx 0$ after around 1 ps. An analysis of the data collected at delay times $t > 2\,\mathrm{ps}$, when the amplitude of the driving pulse has returned to nearly zero, gives access to the undriven coherent vibrational dynamics of the sample (see Fig. 2(d)). The measured mode frequencies $E'_{\mathrm{TO}} = 2.77 \pm 0.01\,\mathrm{THz}$ and $E''_{\mathrm{TO}} = 4.22 \pm 0.01\,\mathrm{THz}$ are in agreement with Raman measurements, the damping times $(t_{\mathrm{damp}}(E'_{\mathrm{TO}}) \approx 5\,\mathrm{ps}$, $t_{\mathrm{damp}}(E''_{\mathrm{TO}}) \approx 8\,\mathrm{ps})$ are slightly lower than damping times measured in an ISRS measurement.[21]

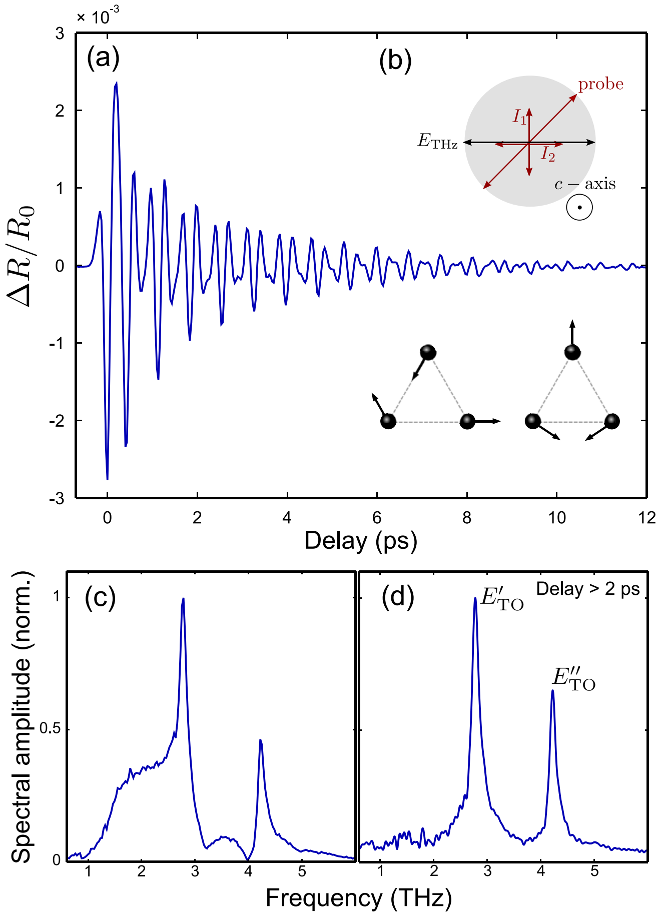

FIG. 2. (a) Changes of anisotropic reflectivity $\Delta R/R_0$ caused by E-symmetry lattice modes resonantly driven by the THz pump pulse E_{THz} are depicted in Fig. 1(b)). (b) Relative polarization of E_{THz} and probe pulses on the Te sample. The lower inset shows the movement of the three atoms in the primitive Te after THz excitation, projected onto a plane perpendicular to the c-axis. (c) Spectral amplitude of the signal obtained via a Fourier transform. (d) Spectral amplitude of the signal for delays $t > 2\,\mathrm{ps}$, when $E_{\mathrm{THz}} \approx 0$. The peaks in the spectrum can be identified as TO non-fully symmetric lattice modes.

To understand the measured reflectivity traces for all delay times, we model the system as a sum of damped harmonic oscillators driven by the electric field of the THz pulse. In the $E \perp c$ geometry, we expect strong coupling only to TO-modes. The equation of motion for a displacement $Q_i(t)$ along the eigenvectors of these modes $(i = E'_{\mathrm{TO}}/E''_{\mathrm{TO}})$ is given by

$$\frac{\partial^2 Q_i(t)}{\partial t^2} + 2\gamma_i \frac{\partial Q_i(t)}{\partial t} + \omega_i^2 Q_i(t) = \frac{q_i^*}{m_i^*} E_{\mathrm{THz}}^T(t), \tag{1}$$

where γ_i and $\omega_i = 2\pi\nu_i$ are the damping constant and angular frequency, q_i^* and m_i^* are effective charge and mass of mode i. The driving force is given by $E_{\mathrm{THz}}^T(\nu) = T(\nu)E_{\mathrm{THz}}(\nu)$, the electric field transmitted into the crystal. Here, $E_{\mathrm{THz}}^T(\nu)$ is the Fourier transform of $E_{\mathrm{THz}}^T(t)$. Our approach is valid for homogeneous excitation of the probed volume of the Te crystal, which is a reasonable assumption since the penetration depth of the THz electric field ($\lambda_{\mathrm{THz}} \approx 2\,\mu$m at the E'_{TO} resonance[28]) is much larger than the optical penetration depth of around 50 nm.[1] The transmission coefficient $T(\nu)$ is strongly frequency-dependent around lattice resonances. We use a Lorentz model approach[29] to calculate the real and imaginary part of the refractive index $n(\nu)$ and $k(\nu)$, as well as $T(\nu)$

$$n^2(\nu) - k^2(\nu) = \varepsilon_0 + \sum_i 4\pi\rho_i\nu_i^2 \frac{\nu_i^2 - \nu^2}{\left(\nu_i^2 - \nu^2\right)^2 + \left(\gamma_i\nu_i/(2\pi)\right)^2},$$

$$n(\nu)k(\nu) = \sum_i \rho_i\nu_i^2 \frac{\gamma_i\nu_i}{\left(\nu_i^2 - \nu^2\right)^2 + \left(\gamma_i\nu_i/(2\pi)\right)^2},$$

$$T(\nu) = \frac{2}{1 + n(\nu) + ik(\nu)}.$$

Here, ε_0 is the high-frequency dielectric constant and ρ_i is related to the oscillator strength.[29] Assuming a flat frequency response of the GaP detection crystal in the relevant frequency range, we employ the measured THz pulse as a driving field and use $T(\nu)$ to calculate the field inside the crystal. The relative magnitude of the measured spectral amplitudes of different modes is determined by two parameters. First, the coupling of lattice modes to a driving field E^T_{THz}, which is set by the effective dynamic charge and the effective mass associated with a certain mode. Second, the change in anisotropic reflectivity associated with a displacement amplitude Q, which is determined by elements of the Raman tensor $(\partial\chi/\partial Q)_{uv}$ via $\Delta R = (\partial\chi/\partial Q)_{uv}E_u^{(1)}E_vQ - (\partial\chi/\partial Q)_{uv}E_u^{(2)}E_vQ$, where $E_u^{(1)}$ and $E_u^{(2)}$ are the reflected probe fields with orthogonal polarization and E_v is the incident probe field.[21] For E-symmetry modes $(\partial\chi/\partial Q)_{uv}$ has nondiagonal components, resulting in an anisotropic reflectivity change. In the model, we use one fitting parameter that determines the relative spectral amplitude. For known effective dynamic charge and mass, we can therefore estimate the relative detection sensitivity given by the Raman tensor for a specific experimental geometry.

The relative magnitude of measured resonance peaks is furthermore modified by the experimental time resolution, which we account for by convolving the solutions of the equation of motion with a Gaussian.

A fit to the data is shown in Fig. 3. The retrieved values from the fit $\nu_{E'_{\mathrm{TO}}}$=2.78±0.02THz,$\nu_{E''_{\mathrm{TO}}}$=4.23±0.03THz,$\gamma_{E'_{\mathrm{TO}}}$=0.36±0.07THz and $\gamma_{E''_{\mathrm{TO}}}$=0.34±0.1THz agree well with values retrieved from the mode spectrum of the undriven motion for time delays $t>2$ps (see Fig. 2(d)). The simple harmonic oscillator model reproduces well the shape of the spectral amplitude of the lower frequency E'_{TO} mode, while it fails to capture the full structure around the E''_{TO} peak. The measured broad peak corresponding to a strongly damped mode centered at around 3.6 THz could be related to an extraordinary phonon mode[30] or background signal related to a linear EO effect.[31] To test if any nonlinear coupling between modes is observable in the spectrum, we varied the THz field strength by varying the relative orientations of two wiregrid polarizers placed in the THz beam path. No change in the measured spectrum over a wide range of THz field strengths could be observed. Using values for the effective dynamic charge from Lucovsky[32] and assuming an equal effective mass, the ratio of the Raman detection sensitivity in this geometry yields $E''_{\mathrm{TO}}/E'_{\mathrm{TO}} \approx 14$. The fact that the high frequency shoulder of the E''_{TO} is not fully reproduced by the fit could be related to the decreasing sensitivity of our EO detection system for frequencies near 5 THz,[33] since we use the measured THz trace as a driving field.

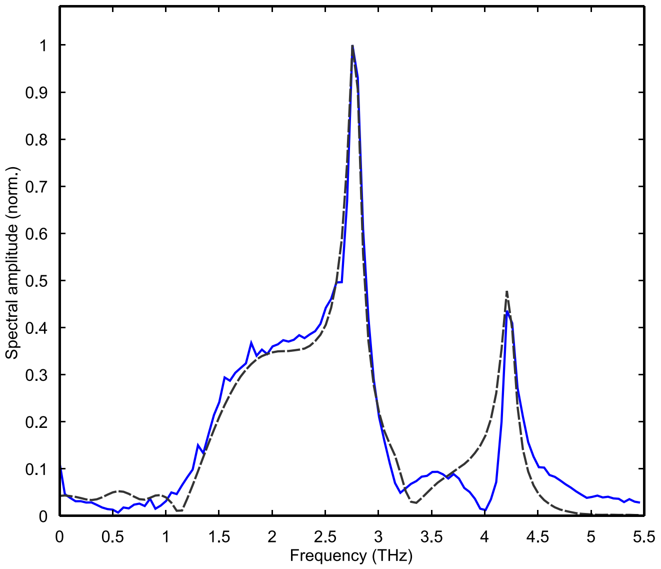

FIG. 3. Fit of the driven harmonic oscillator model as described in the text to the data. Blue line: FFT of measured anisotropic reflectivity change. Dashed line: Harmonic oscillator model.

In summary, we used intense pulses of THz electromagnetic radiation to resonantly excite non-fully symmetric lattice modes in single crystal Te. The demonstrated approach can have advantages to other time-resolved spectroscopic techniques like THz TDS and above-bandgap ISRS, given that the probe process relies on optical laser pulses and no electron-hole pairs are generated by the pump. With the demonstrated experimental setup, the combination of intense THz pulses generated via optical rectification of an OPA beam and using the fundamental laser pulses for probing the coherent structural motion allows us to achieve a high signal-to-noise ratio. The method is, however, restricted to the study of excitations that are both IR active and Raman active, consequently limiting the systems to ones without a spatial inversion center. When strongly damped modes are present, it can also become difficult to disentangle the spectrum of the THz pulse and the material response and precise knowledge of spectral components of the driving field is necessary to understand the data. While at field strengths of around 0.6 MV/cm a large-amplitude coherent motion was excited, no anharmonic coupling of different lattice modes could be observed. Further advances in generation methods may offer unique opportunities to explore anharmonic coupling in the low THz regime in a similar experimental setting.

We acknowledge financial support by the NCCR Molecular Ultrafast Science and Technology (NCCR MUST), a research instrument of the Swiss National Science Foundation (SNSF).

[1] S. Hunsche, K. Wienecke, T. Dekorsy, and H. Kurz, Phys. Rev. Lett. **75**, 1815–1818 (1995).

[2] T. Dekorsy, G. Cho, and H. Kurz, "Light Scattering in Solids VIII," in *Millimeter and Submillimeter Save Spectroscopy of Solids* (Springer, Heidelberg, 2000), p. 169.

[3] S. Wall, D. Wegkamp, L. Foglia, K. Appavoo, J. Nag, R. F. Haglund, J. Stähler, and M. Wolf, Nat. Commun. **3**, 721 (2012).

[4] S. O. Mariager, A. Caviezel, P. Beaud, C. Quitmann, and G. Ingold, Appl. Phys. Lett. **100**, 261911 (2012).

[5] H. Schäfer, V. V. Kabanov, M. Beyer, K. Biljakovic, and J. Demsar, Phys. Rev. Lett. **105**, 066402 (2010).

[6] R. Yusupov, T. Mertelj, V. V. Kabanov, S. Brazovskii, P. Kusar, J.-H. Chu, I. R. Fisher, and D. Mihailovic, Nat. Phys. **6**, 681–684 (2010).

[7] T. Huber, S. Mariager, A. Ferrer, H. Schäfer, J. Johnson, S. Grübel, A. Lübcke, L. Huber, T. Kubacka, C. Dornes, C. Laulhe, S. Ravy, G. Ingold, P. Beaud, J. Demsar, and S. Johnson, Phys. Rev. Lett. **113**, 026401 (2014).

[8] H. Zeiger, J. Vidal, T. Cheng, E. Ippen, G. Dresselhaus, and M. Dresselhaus, Phys. Rev. B **45**, 768 (1992).

[9] T. Stevens, J. Kuhl, and R. Merlin, Phys. Rev. B **65**, 144304 (2002).

[10] H. Hirori, F. Blanchard, and K. Tanaka, Appl. Phys. Lett **98**, 091106 (2011).

[11] C. P. Hauri, C. Ruchert, C. Vicario, and F. Ardana, Appl. Phys. Lett. **99**, 161116 (2011).

[12] T. Kampfrath, A. Sell, G. Klatt, A. Pashkin, S. Mährlein, T. Dekorsy, M. Wolf, M. Fiebig, A. Leitenstorfer, and R. Huber, Nat. Photonics **5**, 31–34 (2011).

[13] T. Kubacka, J. A. Johnson, M. C. Hoffmann, C. Vicario, S. de Jong, P. Beaud, S. Grübel, S.-W. Huang, L. Huber, L. Patthey, Y.-D. Chuang, J. J. Turner, G. L. Dakovski, W.-S. Lee, M. P. Minitti, W. Schlotter, R. G. Moore, C. P. Hauri, S. M. Koohpayeh, V. Scagnoli, G. Ingold, S. L. Johnson, and U. Staub, Science **343**, 1333–1336 (2014).

[14] M. C. Nuss and J. Orenstein, "Terahertz time-domain spectroscopy," in *Millimeter and Submillimeter Wave Spectroscopy of Solids* (Springer, 1998), pp. 7–50.

[15] A. Pashkin, M. Kempa, H. Nemec, F. Kadlec, and P. Kuel, Rev. Sci. Instrum. **74**, 4711–4717 (2003).

[16] M. Stillhart, A. Schneider, and P. Günter, J. Opt. Soc. Am. B **25**, 1914–1919 (2008).

[17] P. Grosse, *Die Festkörpereigenschaften von Tellur*, Springer Tracts in Modern Physics Vol. 48 (Springer Berlin/Heidelberg, 1969).

[18] C. Adenis, V. Langer, and O. Lindqvist, Acta Crystallogr., Sect. C **45**, 941–942 (1989).

[19] I. Chen and R. Zallen, Phys. Rev. **173**, 833–843 (1968).

[20] T. Cheng, J. Vidal, H. Zeiger, G. Dresselhaus, M. Dresselhaus, and E. Ippen, Appl. Phys. Lett. **59**, 1923–1925 (1991).

[21] T. Dekorsy, H. Auer, C. Waschke, H. J. Bakker, H. G. Roskos, H. Kurz, V. Wagner, and P. Grosse, Phys. Rev. Lett. **74**, 738–741 (1995).

[22] S. Johnson, E. Vorobeva, P. Beaud, C. Milne, and G. Ingold, Phys. Rev. Lett **103**, 205501 (2009).

[23] P. C. M. Planken, H.-K. Nienhuys, H. J. Bakker, and T. Wenckebach, J. Opt. Soc. Am. B **18**, 313–317 (2001).

[24] D. E. Aspnes and A. A. Studna, Phys. Rev. B **27**, 985–1009 (1983).

[25] B. Yu, S. Machavariani, A. Natsvlishvili, and A. Chirakadze, J. Phys. D: Appl. Phys. **22**, 682 (1989).

[26] Q. Wu and X. C. Zhang, Appl. Phys. Lett. **70**, 1784–1786 (1997).

[27] The calculated error originates from pump and probe fluctuations; an uncertainty estimate for parameters taken from literature is omitted. The calculated field value represents a lower bound since some experimental conditions that would decrease the measured field (beam divergences, etc.) are not accounted for.

[28] Calculated with reflectivity data from Ref. 32.

[29] W. Spitzer and D. Kleinman, Phys. Rev. **121**, 1324 (1961).

[30] W. Richter, J. Phys. Chem. Solids **33**, 2123–2128 (1972).

[31] C. Hammond, J. Jenkins, and C. Stanley, Opto-electronics **4**, 189–196 (1972).

[32] G. Lucovsky, R. C. Keezer, and E. Burstein, Solid State Commun. **5**, 439–445 (1967).

[33] A. Leitenstorfer, S. Hunsche, J. Shah, M. C. Nuss, and W. H. Knox, Appl. Phys. Lett. **74**, 1516–1518 (1999).